TWO MODELS OF DUCTILE FRACTURE IN CONTEST: POROUS METAL PLASTICITY AND COHESIVE ELEMENTS

Thomas Siegmund, Günter Bernauer and Wolfgang Brocks

The present paper reviews computational models for the analysis of ductile fracture. The computational models use local criteria for material separation: either the Gurson-Tvergaard-Needleman model incorporating void nucleation, growth and coalescence or a more phenomenological cohesive zone model. Results from computations using these models are presented and compared to experiments. The capabilities of the two models for material failure are compared and discussed. Relationships between the parameter sets are outlined. Finally, an improved cohesive zone model is introduced that captures the effects of the stress triaxiality on material separation.

INTRODUCTION

In ductile fracture the fracture process zone can be identified with the region where the loss of material strength due to growth and link-up of voids is larger than the strain hardening. For the analysis of crack growth it is thus necessary to introduce constitutive relations covering the effect of the loss of stress carrying capacity.
This approach also allows to explore relationships between the macroscopic toughness of a specimen, the dissipation in the plastic zone and the work of separation itself. In a computational framework two types of approaches are discussed in the following and their results are compared to each other and to experimental data on crack growth resistance.
The use of the Gurson-Tvergaard-Needleman (GTN) model for the prediction of ductile fracture is, today, widely accepted (1-4). Thereby, the material separation characteristics are the result of the process of void growth and nucleation as well as coalescence.

Institute of Materials Research, GKSS Research Center, D-21502 Geesthacht, Germany

The set of equations for the GTN-model includes a flow potential (Eq. 1), relations for void evolution (Eq. 2, 3) and void coalescence (Eq. 4). These relations are summarized in the following:

$$\phi = \left(\frac{\sigma_e}{\sigma_M}\right)^2 + 2q_1 f^* \cosh\left(\frac{3}{2}\frac{q_2\sigma_h}{\sigma_M}\right) - \left[1 + q_3(f^*)^2\right] = 0 \quad , \tag{1}$$

$$\dot{f} = \dot{f}_{growth} + \dot{f}_{nuc} \quad , \quad \dot{f}_{growth} = (1-f)\dot{\epsilon}_{ij}^{pl}\delta_{ij} \quad , \quad \dot{f}_{nuc} = A\dot{\bar{\epsilon}}_M^{pl} \quad , \tag{2}$$

$$A = \frac{f_N}{s_N\sqrt{2\pi}} \exp\left\{-\frac{1}{2}\left[\frac{\bar{\epsilon}_M^{pl} - \epsilon_N}{s_N}\right]^2\right\} \quad , \tag{3}$$

$$f^*(f) = f \quad \text{for} \quad f \leq f_c \quad \text{and} \quad f^*(f) = f_c + k(f - f_c) \quad \text{for} \quad f > f_c \tag{4}$$

The material parameters to be determined are those describing the continuum surrounding the void (the elastic constants E, ν, the plastic deformation behavior $\sigma_M(\epsilon_p)$), the initial void volume (f_0), the void nucleation (f_n, ϵ_n, s_N), the void growth (q_1, q_2, q_3) and finally the void coalescence (f_c, k). In addition, the use of this strain softening constitutive relations must be combined with a lengthscale, D, to resolve the issue of localization. In most engineering applications of the GTN-model D is equal to the size of the elements in front of the crack tip. The lengthscale then represents the height of the fracture process zone and often is assumed to be in the range of several hundreds of micrometers. This approach implies that the mesh design for the fracture mechanics specimen under consideration has to be based on this length scale and thus does not allow for arbitrary mesh refinements. This argument and the rather large number of material parameters to be determined are the key issues in an engineering application of the GTN-model.

Several of the difficulties of the GTN-model can be by-passed by the use of so called "cohesive zone" models (CZM) (5-9). Here, the material separation characteristics are embedded in special finite elements. These elements possess a fixed inscribed relationship connecting the crack opening displacements with the opening stresses. One possible relationship for modeling mode-I crack growth is (5):

$$\sigma_n = \sigma_{max} \mathrm{e} \mathrm{z} \frac{u_n}{\delta} \exp(-\mathrm{z}\frac{u_n}{\delta}) \quad , \quad \mathrm{e} = \exp(1) \quad , \quad \mathrm{z} = \frac{16\mathrm{e}}{9} \quad . \tag{5}$$

Besides the specific shape function (Eq. 5) describing the material separation this approach comprises only two material parameters (6): the cohesive strength, σ_{max}, and the cohesive length, δ. The material length scale, δ, is embedded within the cohesive elements so no further introduction of a lengthscale linked to the finite element mesh becomes necessary.

In most applications of cohesive zone models for ductile fracture the two material parameters, σ_{max} and δ, were assumed to be material constants. This approach, however, neglects that the underlying processes of void nucleation, growth and coalescence are dependent on the stress triaxiality imposed on a material element (10). To incorporate the effects of local constraint now both, the cohesive strength and the cohesive length, are introduced as being dependent on the stress triaxiality (11).

This is achieved by transporting the values of the triaxiality of the continuum field into the cohesive elements. Through this coupling the cohesive zone model can become more physically motivated (12).

MODEL SET-UP

The models for material separation presented in the previous section were applied to calculate crack growth in a M(T) ($w = 50$mm, $a_0/w = 0.5$) and C(T) ($w = 50$mm, $a_0/w = 0.59$) specimen. The specimens were made of a ferritic steel with german designation StE460 (2). Crack growth experiments for this steel were performed at the German Federal Institute of Materials Testing, BAM, Berlin (13).
The material parameters in the calculations using the GTN-model are: $f_0 = 0.0025$, $f_N = 0.02$, $\epsilon_N = 0.3$, $s_N = 0.1$, $q_1 = 1.5$, $q_2 = 1.0$, $q_3 = 2.25$, $f_c = 0.021$, $k = 3.4$, $D = 0.2$mm (14). The plastic flow properties for the GTN-model are taken from the true stress-strain curve of the steel under investigation. The near tip mesh design for the GTN-model is depicted in Figure 1a. Only the single row of elements directly in front of the initial crack tip is assigned to the GTN-model. The remaining part of the specimen is modeled as a material following the J_2–flow theory. Its elastic and plastic properties are taken to be identical to those of the matrix material surrounding the voids in the fracture process zone.

For the cohesive zone model using constant values for the cohesive zone parameters the best agreement between experiments and computational predictions was achieved by using the values:

$$\sigma_{max}/\sigma_0 = 3.36 \quad , \quad \delta/D = 0.3 \tag{6}$$

The cohesive zone parameters for the triaxiality dependent cohesive zone model were determined by unit cell calculations (11). Material unit cells with their effective behavior being described by the GTN-model were loaded under constant applied stress ratios. The resulting dependencies of the cohesive zone parameters on the triaxiality value, T, in the vicinity of the crack tip read:

$$\sigma_{max}/\sigma_0 = -4.8 \exp\left(-\frac{\max(T) + 0.032}{0.52}\right) + 3.56 \quad , \tag{7}$$

$$\delta/D = 1.34 \exp\left(-\frac{\max(T) - 0.45}{0.89}\right) + 0.13 \tag{8}$$

Again, the remaining part of the specimen is modeled as a material which follows the J_2–flow theory.
The mesh design in the near tip region for the use of the cohesive zone model is depicted in Figure 1b. Both, the GTN as well as the CZM calculations used 4 node quadrilateral plane strain finite elements. Figure 2 schematically depicts the coupling of the triaxiality in the continuum to the cohesive zone elements.

RESULTS

First, the global specimen behavior is investigated. This is done by analyzing the crack growth resistance as given by the relationship between J and Δa. Figure 3 now depicts the crack growth resistance as determined in the experiments and by the computations. All three models are suitable to allow computations of the experimentally determined crack extensions up to $\Delta a = 8$mm.
The experimentally determined crack growth resistance is strongly dependent on the specimen geometry. This effect is captured quite well by the use of all three models of material separation. The predictions of the GTN-model are in very good agreement with the experiments for both the M(T) and C(T) specimen. For the cohesive zone models the predictions of the crack growth resistance shows some deviations from the experimentally determined values in the case of the M(T) specimen.

For a detailed understanding and evaluation of the fracture processes it is, in addition, of interest to evaluate the material separation behavior at the crack tip. This part of the specimen response is not directly accessible by experiments. Computational modeling of fracture by use of micromechanics based constitutive equations can, however, provide an insight into local quantities at the crack tip. Here, the material separation behavior is investigated at the location $\Delta a = 4$mm. At this location a steady state of the relation between the opening stress and the displacement jump across the crack surfaces has already been reached. Figure 4 depicts the material separation behavior for the M(T) and C(T) specimen as predicted by the GTN-model, the cohesive zone model with constant material data and with triaxiality dependent material data. The physically process based GTN-model clearly predicts a material separation behavior for the C(T) specimen different from that in the M(T) specimen. While the peak stresses reached in both specimens are similar the displacement after which the stress falls to zero is nearly twice as large in the M(T) specimen compared to the C(T) specimen.
The geometry dependence of the material separation in the fracture process zone cannot be captured by the use of the cohesive zone model with constant material parameters. In this case, the material separation is independent of the specimen geometry. Introducing, however, σ_{max} and δ as dependent on the triaxiality the predictions improve considerably and a geometry dependence of the material separation is again predicted. As seen from Figure 4 the predictions of the material separation from the new triaxiality dependent cohesive zone model are in very good agreement with those from the GTN-model.

CONCLUSION

Ductile crack growth in a mild steel was investigated using the GTN-model as well as cohesive cohesive zone models with constant and with triaxiality dependent material parameters.
On the global specimen level, where mainly the plastic deformation outside the fracture process zone counts, all three approaches predict the geometry dependence of the crack growth resistance, described by the J–Δa curve, equally well. The

predictions are in good agreement with the experimentally determined values. A geometry dependent behavior of the material in the fracture process zone can only be described by using the GTN-model and the new cohesive zone model with triaxiality dependent material parameters. The use of the classical approach to cohesive zone models with constant material parameters lacks this variability and describes the material behavior in the fracture process zone in an average sense.

REFERENCE

(1) Needleman, A., and Tvergaard, V., J. Mech. Phys. Solids, Vol. 35, 1987, pp. 151-183.

(2) Brocks, W., Klingbeil, D., Künecke, G., and Sun, D.-Z., "Application of the Gurson model to ductile tearing resistance." In Proceedings of ASTM-meeting "Constraint effects in fracture: Theory and applications." Edited by M. Kirk and A. Bakker, ASTM STP 144, 1995.

(3) Xia, L., Shih, C.F., and Hutchinson, J.W., J. Mech. Phys. Solids, Vol. 43, 1995, pp. 389-413.

(4) Ruggieri, C., Dodds, R.H., and Panontin, T.L., Int. J. Fract., Vol. 82, 1996, pp. 67-95.

(5) Needleman, A., Int. J. Fract., Vol. 42, 1990, pp. 21-40.

(6) Tvergaard, V., and Hutchinson, J.W., J. Mech. Phys. Solids, Vol. 40, 1992, pp. 1377-1397.

(7) Tvergaard, V., and Hutchinson, J.W., Int. J. Solids Structures, Vol. 31, 1994, pp. 823-833.

(8) Siegmund, T., and Needleman, A., Int. J. Solids Structures, Vol. 43, 1997, pp. 769-787.

(9) Lin, G., Kim, Y.-J., Cornec, A., and Schwalbe, K.-H., Comp. Mat. Sci., Vol. 9, 1997, pp. 36-47.

(10) Koplik, J., and Needleman, A., Int. J. Solids Structures, Vol. 24, 1988, pp. 835-853.

(11) Siegmund, T., and Brocks, W., J. de Physique IV, Proceedings EURMECH-MECAMAT' 98, in print.

(12) Tvergaard, V., and Hutchinson, J.W., Int. J. Solids Structures, Vol. 33, 1996, pp. 3297-3308.

(13) Häcker, R., Gerwien, P., Thiemich, K.-D., Wossidlo, P., and Baer, W., German Federal Institute of Material Testing, Report No. BAM-V.33 98/2, 1998.

(14) Klingbeil, D., Künecke, G., and Schicker, J., German Federal Institute of Material Testing, Report No. BAM-1.31 93/3, 1993.

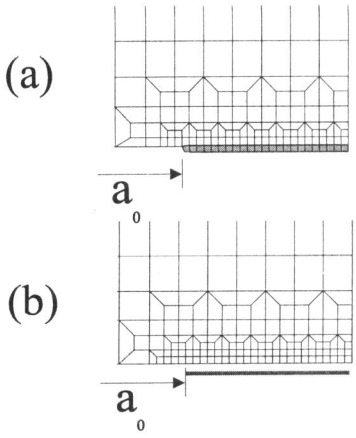

Figure 1 Mesh design at the crack tip for (a) the GTN-model, (b) the CZM.

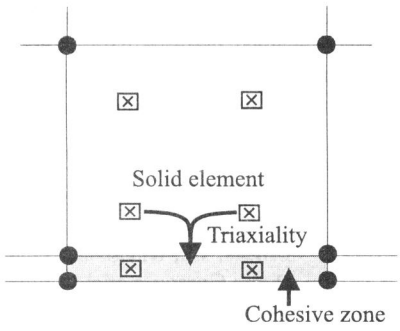

Figure 2 Schematic drawing of the coupling in the triaxiality dependent CZM.

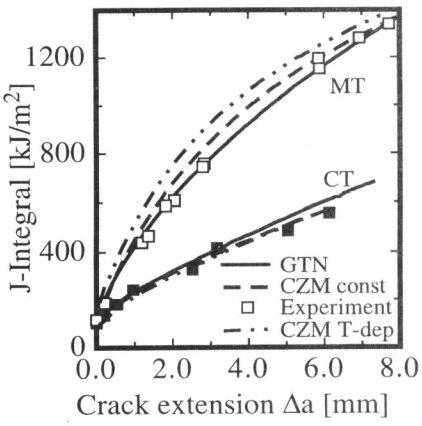

Figure 3 J–Δa curves; experiments and computations.

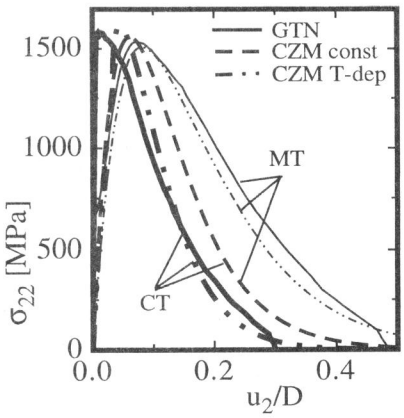

Figure 4 Predictions of the material separation behavior.